Treatment of Multiple Beam X-ray Diffraction in Energy Dependent Measurements

Melanie Nentwich,[a]* Matthias Zschornak,[b] Tina Weigel,[b]
Thomas Köhler,[b] Dmitri Novikov,[a] Dirk C. Meyer[b] and
Carsten Richter[c]

[a]*Deutsches Elektronen-Synchrotron DESY, Notkestr. 85, 22607 Hamburg Germany,* [b]*Institute of Experimental Physics, Technical University Bergakademie Freiberg, 09596 Freiberg, Germany, and* [c]*Leibniz-Institut für Kristallzüchtung, Max-Born-Straße 2, 12489, Berlin, Germany. E-mail: Melanie.Nentwich@desy.de*

Resonant Elastic X-ray Scattering; **Multiple Beam X-ray Diffraction**; **Renninger Effect**; **Data Processing**

Abstract

During X-ray Diffraction experiments on single crystals, the diffracted beam intensities may be affected by *Multiple Beam X-ray Diffraction* (MBD). This effect is particularly frequent at higher X-ray energies and for larger unit cells. The appearance of this so-called *Renninger Effect* often impairs the interpretation of diffracted intensities. This applies in particular to energy spectra analysed in resonant experiments since during scans of the incident photon energy these conditions are necessarily met for specific X-ray energies. This effect can be addressed by carefully avoiding multiple beam reflection conditions at a given X-ray energy and a given position in reciprocal space. However, the areas, which are (nearly) free of MBD are not always available. This article presents a universal concept of data acquisition and post processing for

resonant X-ray diffraction experiments. Our concept facilitates the reliable determination of kinematic (MBD-free) resonant diffraction intensities even at relatively high energies, which, in turn, enables the study of higher absorption edges. This way, the applicability of resonant diffraction, e.g. to reveal the local atomic and electronic structure or chemical environment, is extended for a vast majority of crystalline materials. The potential of this approach in comparison to conventional data reduction is demonstrated on measurements of the Ta L_3 edge of well-studied lithium tantalate $LiTaO_3$.

1. Introduction

X-ray Diffraction (XRD) from perfect single crystals is described by the dynamical theory of diffraction [1, 2]. It also describes the interference effects that appear when the Bragg condition is fulfilled for several reflections. This so-called *Multiple Beam X-ray Diffraction* (MBD) may result in enhancement or dampening of diffracted intensity [3–7]. In contrast, the diffraction from slightly imperfect or small crystals can be described by the kinematic theory of diffraction, as small lattice coherence length prevents the multiple wave interference effect to a large extent [8–10]. Most practical applications assume the kinematic approach to be valid and dynamical effects are treated as a source of experimental error. However, especially for hard X-rays, large unit cells, and weak or even 'forbidden' reflections the measured intensities can be dominated by MBD [11], also called *Renninger Effect* [4] or *Umweganregung*. The investigation of the fine structure oscillations in *Resonant Elastic X-ray Spectroscopy* (REXS) experiments [12–14] suffers particularly from these effects (see Sec. 2), which were either overseen or perceived as disturbing and hence avoided [15–18]. Lately, increasing concomitant interpretation facilitates additional information about the material [19–26]. So-called Renninger scans, describing a rotation about the azimuth angle ψ (about the normal of the diffracting lattice planes), reflect the symmetry of the crystal structure

and bear information about orientation of local electronic orbitals in REXS experiments [27]. Still, the undesired appearance of MBD needs to be carefully handled to obtain clean values of the structure amplitude for data evaluation. One approach is simply avoiding the constellations where this effect occurs, but, as we will show, this is only rarely possible. Thus, here we present an approach how to correct for MBD in a perfectly automatable way.

Recently, Kozlovskaya et al. [28] presented an approach to avoid MBD *a priori*. In advance to the measurements, they calculated so-called Renninger maps displaying the intensity depending on both X-ray energy and azimuthal angle ψ [26, 29–32]. Based on these maps, they determined sample orientations for which the desired energy scan of TeO_2 at approx. 4.94 keV (Te L_1 edge) was free of MBD.

However elegant this approach is, it may not always be applicable. Especially for large ratios of unit cell dimensions to wavelength, the number of reflections close to the Ewald sphere may become too high [16]. Given a compound of interest, the cell dimensions are fixed and solely the photon energy determines this density. As an example, Fig. 1 shows the influence of the energy on the calculated azimuthal dependence of the 'forbidden' 0 3 15 reflection intensity of ferroelectric lithium tantalate $LiTaO_3$. It can be seen that, although the $LiTaO_3$ unit cell is still rather small and X-ray energies of 9.88 keV (Ta L_3 edge) is moderate, hardly any azimuthal range remains unaffected by MBD. Fig. 1 is based on the structure solution of ICSD 9537 [33] and on the equations given in [26] implemented in the python module pyasf [31]. Trigonal lithium tantalate is a well-studied material in regard to structure [33], electrical and chemical properties [34–37], growth [38–41], and defects [42–45] and serves as a model material here.

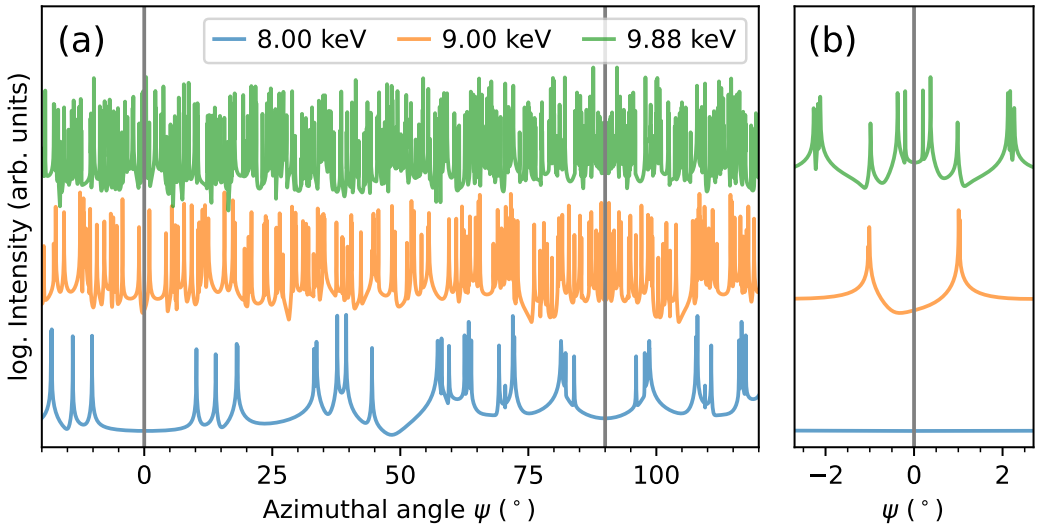

Fig. 1. Simulation of MBD during an azimuthal rotation at different fixed energies, exemplarily for the 'forbidden' 0 3 15 reflection of stoichiometric $LiTaO_3$. Subfigure (b) gives a detailed view of the MBD in form of a zoom-in of the high-symmetric position at $\psi = 0°$. The addition of an intensity offset allows better visualisation.

Evidently, the approach of *a priori* calculations to avoid the occurrence of MBD in the measurements is limited in its application, when the Ewald sphere becomes large. In this work, we present an alternative approach to obtain resonant diffraction spectra free from the Renninger Effect, which facilitates the investigation of a larger group of materials even at higher energy absorption edges. In Sec. 3, we describe the concept of data acquisition and post processing of REXS data and Sec. 4 demonstrates the application of this approach to the aforementioned measurements of $LiTaO_3$.

2. The origin of the Renninger effect

The Renninger Effect was first described by M. Renninger in 1937 when he measured significant intensity at the position of the 'forbidden' 2 2 2 reflection of diamond as it was superimposed by MBD [3]. The effect occurs if two reflections are excited simul-

taneously, *i. e.* when two reciprocal lattice points lie on the Ewald sphere [4] under consideration of the excitation error [26, 46], see Fig. 2 (a). Figure 2 (b) visualises the effect in real space: The diffracted beam $\boldsymbol{k}_1$ is the conventional Bragg reflection of the primary beam $\boldsymbol{k}_0$, caused by diffraction from the blue planes. Simultaneously, $\boldsymbol{k}_0$ is diffracted in a coherent process at another set of crystallographic planes (green) towards $\boldsymbol{k}_2$, which now serves as incoming beam for the red planes, resulting in the diffracted beam $\boldsymbol{k}_3$. In the rare case that $\boldsymbol{k}_3$ points in the same direction as $\boldsymbol{k}_1$, the intensity is either enhanced or damped compared to the signal of $\boldsymbol{k}_1$ alone, depending on the interaction between those beams being constructive or destructive [20]. The conditions to observe the Renninger Effect are related to the Bragg condition of having a second reflection on the Ewald sphere (*i. e.* highly sensitive to lattice parameters, energy, and angular position of the sample). For avoiding or studying the Renninger Effect, the degrees of freedom are the azimuthal rotation (about angle ψ) of the primary reflection or the X-ray energy.

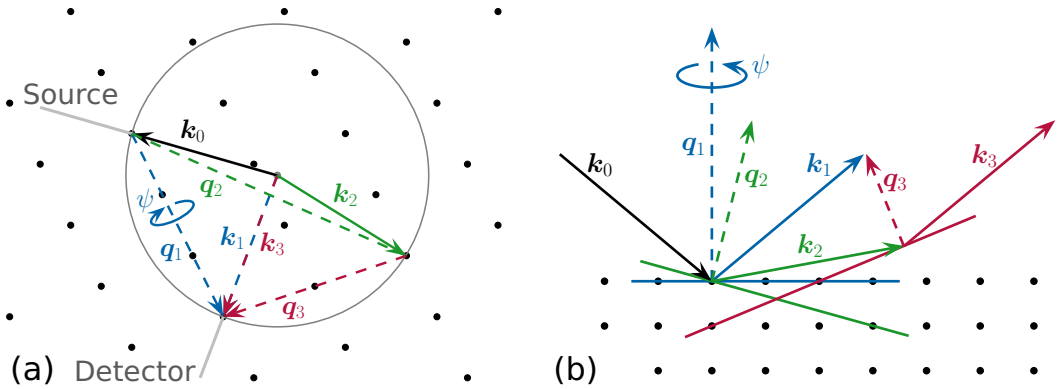

Fig. 2. Principle mechanisms for the appearance of the Renninger Effect. (a) Ewald sphere construction. In addition to the regular Ewald sphere, a third reciprocal lattice point intersects the sphere, indicating an additional diffraction path along reflections $\boldsymbol{q}_2$ and $\boldsymbol{q}_3$ instead of only $\boldsymbol{q}_1$. (b) Real space schematic. The primary beam $\boldsymbol{k}_0$ is diffracted at the blue crystal plane, resulting in the outgoing beam $\boldsymbol{k}_1$ corresponding to reflection $\boldsymbol{q}_1$. At the same time, $\boldsymbol{k}_0$ is also diffracted at the green and red plane. The resulting beams $\boldsymbol{k}_2$ and $\boldsymbol{k}_3$ correspond to the reflections $\boldsymbol{q}_2$ and $\boldsymbol{q}_3$, respectively. $\boldsymbol{k}_1$ and $\boldsymbol{k}_3$ have the same direction as well as energy, thus the intensity of reflection $\boldsymbol{q}_1$ and multiply diffracted reflection $\boldsymbol{q}_3$ are superimpose in a constructive or destructive way.

The azimuthal rotation corresponds to a rotation of the reciprocal lattice around $\boldsymbol{q}_1$ in the Ewald sphere, Fig. 2 (a). Depending on the inclination of $\boldsymbol{q}_2$ with respect to $\boldsymbol{q}_1$, small rotations may cause additional reciprocal lattice points to leave or to enter the surface of this sphere and, thus, to violate or fulfil the Laue condition of the MBD. Therefore, the MBD exhibits a larger or a similar angular width compared to other Bragg reflections. The density of reciprocal lattice points in the vicinity of the surface of the Ewald sphere in Fig. 2 (a) and, thus, the probability to encounter MBD increases with the ratio of unit cell dimensions to wavelength [47].

3. Data Acquisition and Processing

The occurence of the Renninger Effect is practically unavoidable when recording REX spectra, since, usually, scanning a range of incident photon energies is required. One

way to filter out the desired energy dependencies of the two beam case (in the absence of MBD) is to acquire several scans for the same energy range at arbitrarily chosen azimuthal angles, as outlined in Fig. 3. However, the number of required azimuthal positions to obtain a clean spectrum also depends on the choice of these angles. In this case, due to a high number of reciprocal lattice points close to the Ewald sphere surface, the number of scans was not sufficient. The data was recorded in Bragg geometry with the 6-circle Huber diffractometer of beamline P23 of PETRA III synchrotron, Hamburg. The energy resolution of the used Si(111) double crystal monochromator is $\approx 1.3 \times 10^{-4}$. Both the beam divergence and its energy bandwidth influence the visibility and sharpness of MBD during energy scans. With its beam parameters, beamline P23 represents a typical case.

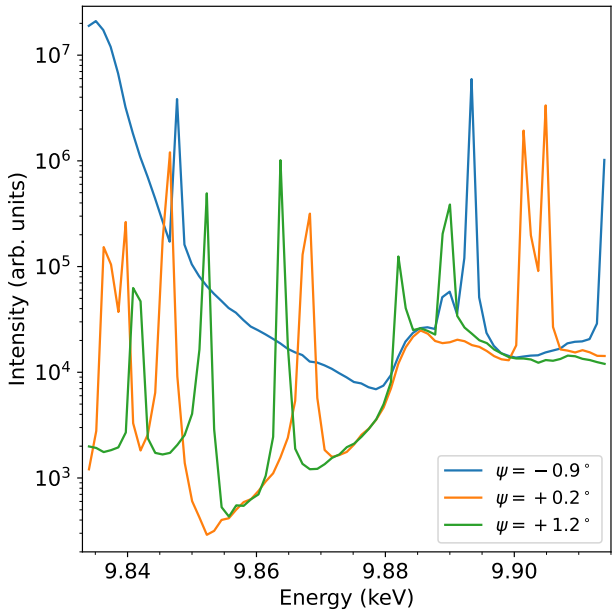

Fig. 3. Experimental energy scans at different azimuthal angles for the 'forbidden' 0 3 15 reflection of congruent $LiTaO_3$ at the Ta L_3 edge.

We were able to improve the quality of the spectra by significantly increasing the data redundancy using a larger number of azimuthal positions (angle ψ, $\approx$ 25 steps, inner

loop) on the expense of a rougher sampling of the photon energy (≈ 75 steps) in the outer loop. In general, the rotation about the azimuthal angle ψ of a given reflection requires a combined rotation about three (*e. g.* Eulerian) axes of the diffractometer unless the diffracting lattice planes can be aligned perpendicular to one of the rotation axes. At optimized beamlines, continuous coupled scans of several axes are nowadays available, allowing to acquire a much higher number of azimuthal data points per time. Using a 2D detector allows to separate background from diffracted signal including MBD. The zero position of the azimuthal needs to be defined (*e. g.* following the convention of Schwarzenbach [48]) and determined for the respective crystal under study as demonstrated in Fig. 4. Here, the measurement settings were such that the inner rotation axis ϕ was nearly parallel to the ψ axis and the high symmetry position at $\phi = 10.23°$ was found as the zero position of ψ.

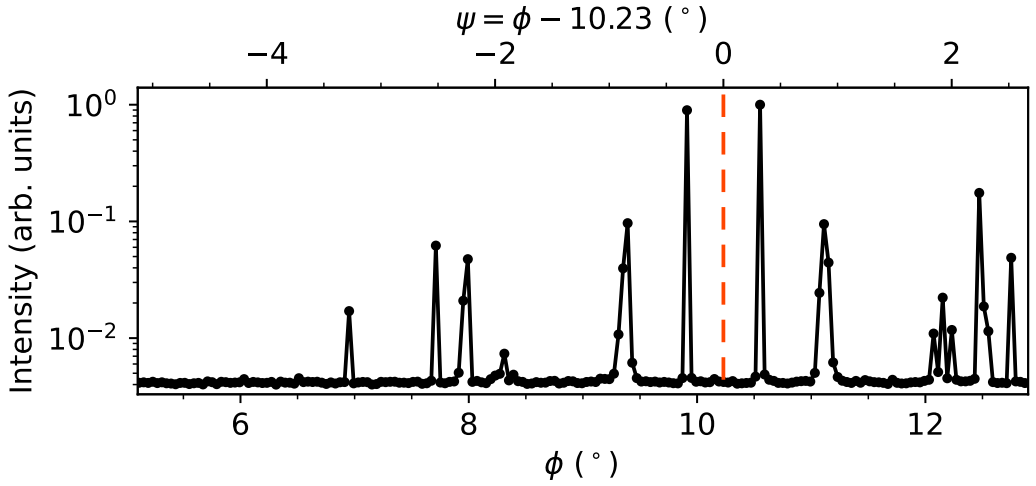

Fig. 4. Experimental azimuthal scan of congruent $LiTaO_3$ at the Ta L_3 edge for the 'forbidden' 0 3 15 reflection realised by rotating ψ/ϕ. The high symmetry position at $\phi = 10.24°$ marks the zero position of the azimuthal ψ with a red line.

To disentangle the individual contributions to a REXS measurement, we additionally

improved the subsequent data analysis with a multilevel routine that takes frames from 2D detectors and was implemented in python code, see Fig. 5 and Supplemental Material S2. The starting point of our approach is that there is no azimuthal position in a Renninger map that is free of MBD. However, we assume that, for each energy, there are azimuthal values where the influence of MBD is negligible. We now want to identify these automatically and use them to create a clean spectrum. In the following paragraph, we will describe this process and the involved data treatment including different corrections (*e. g.* background, detector, incoming beam intensity, ...).

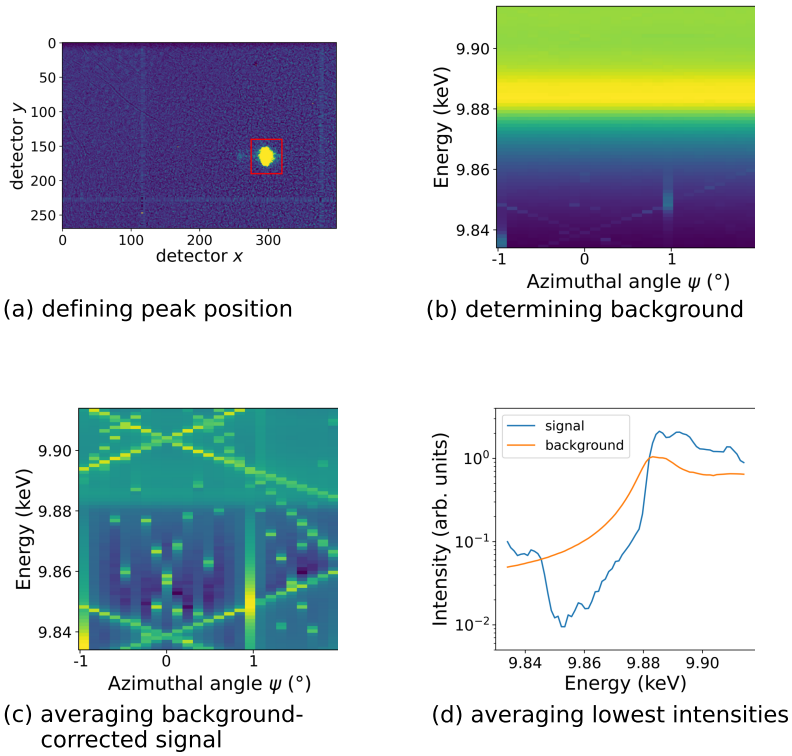

Fig. 5. Stepwise procedure to filter out the Renninger Effect and background leading to the corrected REXS signal. This is exemplarily shown for the 'forbidden' 0 3 15 reflection near the Ta L_3 edge of congruent $LiTaO_3$ from experimental data. The steps include (a) manually defining the peak position on the detector frame, (b) determining background intensity for each detector frame taken within the ψ-E grid, (c) subtracting the background signal for each point of the ψ-E grid, and (d) for each energy averaging lowest intensities from the different azimuthal positions.

The basic idea of the presented approach is that no azimuthal position in a Renninger map exists that is free of MBD. However, a reasonable assumption is that there are azimuthal values where the influence of MBD is negligible (for each energy). We now want to identify these (energy dependent) azimuthal values automatically and use them to create a clean spectrum. In the following paragraph, we will not only describe this process, but also the complete data treatment including different corrections (*e. g.* background, detector, incoming beam intensity, etc.).

The main steps of this routine are visualised in Fig. 5. Once the raw data (detector frames and motor positions) is loaded, the frames are normalized to the primary beam and corrected for detector artifacts caused by differently sensitive pixels (hot and dead pixels) by flatfield correction. In order to separate the background from the actual signal (including MBD) for each of the detector frames, the region containing the diffracted intensity on the detector is marked by the users in step (a). Everything outside this region is considered as constant background for each ψ and E, leading to the map shown in Fig. 5(b). The background-corrected signal is obtained by subtracting the average of the intensity readings outside the user-selected region from the average of those values inside. This is done for each azimuth and X-ray energy leading to the map in Fig. 5(c).

In the last step (d), the Renninger Effect is filtered out by evaluating ψ dependent intensity $I_E(\psi)$ for a given X-ray energy E. In the case of strong, allowed reflections, both an increase and decrease of intensity could falsify the measurement. Thus, the median of $I_E(\psi)$ is interpreted as the MBD-free intensity. An average cannot be used as extremely high MBD-signal will falsify the results. In the case of weak (*e. g.* forbidden) reflections, only an increase in intensity due to MBD is observed. In this case, the lowest intensity values are interpreted as MBD-free. In contrast, the background values are reduced to a 1-dimensional array over energy by averaging the values corresponding to different ψ at the same energy.

4. Results

We exemplarily tested this approach for the 'forbidden' 0 3 15 reflection of a congruent $LiTaO_3$ single crystal (Crystec, Berlin). The spectra of forbidden reflections are particularly prone to MBD contributions, as they are weak. We were able to acquire sufficiently redundant data to extract energy dependent REX spectra that are almost

free from the Renninger Effect. Figure 6 shows the final result of the procedure using ψ-E grid scans (black, as in Fig. 5 (d)) in comparison to the initial E scans (red, as in Fig. 3).

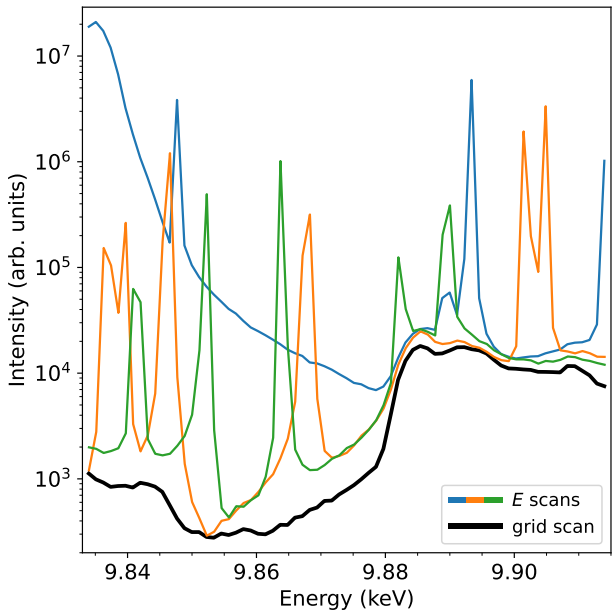

Fig. 6. Experimental comparison between fine E scans at few azimuthal values (blue, orange, green; as in Fig. 3) and ψ-E grid scans (black; as in Fig. 5 (d)), exemplarily for the 0 3 15 reflection of congruent $LiTaO_3$.

To benchmark the data correction procedure (to recover the MBD-free signal), we apply it to a calculated spectrum including MBD. The calculations performed for $LiTaO_3$ are based on the structure solution of ICSD 9537 [33]. The purely energy dependent part and the MBDs were calculated separately employing fdmnes [49] and pyasf [31], respectively, see Fig. 7. As both programs are not interfaced to each other, the data needs to be rescaled to match the experiment. Some discrepancy between calculated and experimental data regarding the MDB-free, ψ-independent part is expected due to an uncertainty in the temperature-induced atomic *Atomic Displacement Parameters* (ADP) [12, 13].

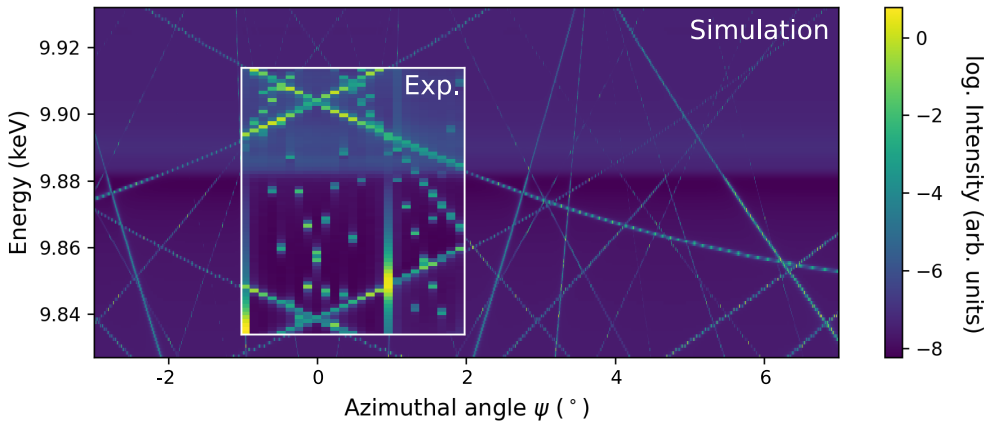

Fig. 7. Overlay of the experimental data onto the simulations with pyasf and fdmnes for the 'forbidden' 0 3 15 reflection at the Ta L_3 edge of congruent $LiTaO_3$. Both simulations taken individually do not provide the complete information required: pyasf [31] delivers the MBD contribution whereas fdmnes [49] delivers the resonant contribution of the 'forbidden' reflection.

Figure 8 demonstrates the influence of the choice of the threshold to discriminate the MDB-affected values to as described above in step (d). We consider again the 'forbidden' 0 3 15 reflection of $LiTaO_3$. At a given X-ray energy E, the threshold is placed at different percentiles (*e. g.* lowest 5 %; with lowest 100 % representing the overall mean of the data). Additionally, we present the overall median (equal to the 50^{th} percentile). The bottom part of Fig. 8 presents the relative differences between original (fdmnes) and restored signal $(I_\text{r} - I_\text{o})/I_\text{o}$, with their averages ranging between 1.2×10^{-2} to 5.7×10^{2}. As expected, for this weak 'forbidden' reflection, the most reasonable choices of threshold for step (d) are the lowest percentiles of up to 10 %.

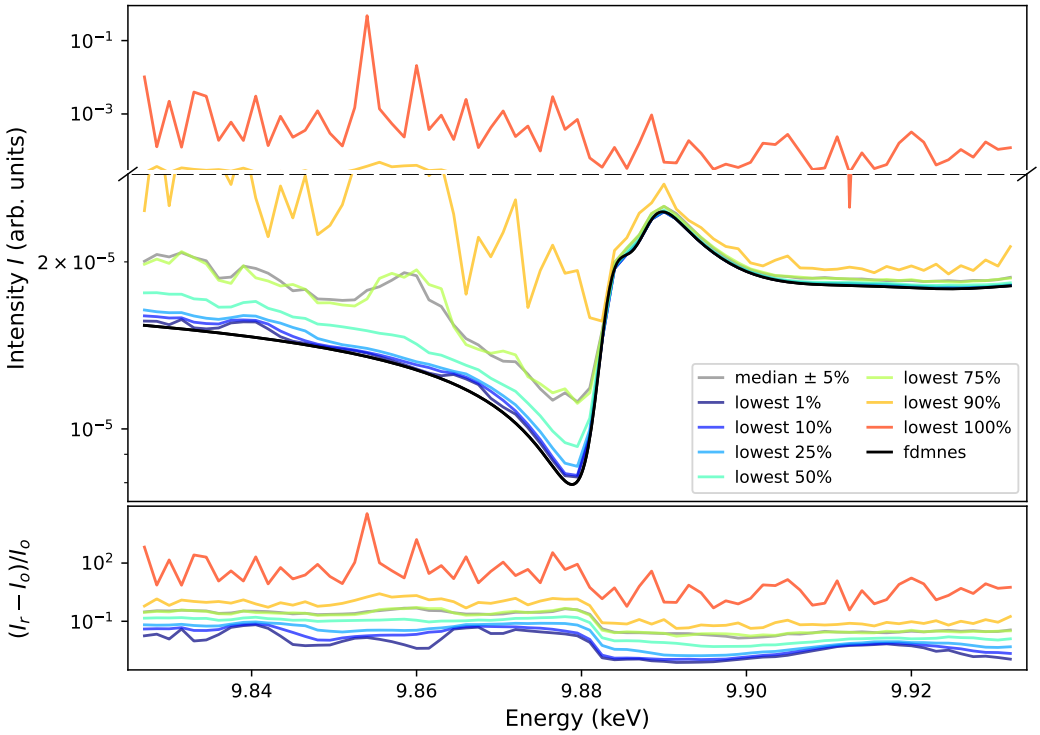

Fig. 8. Top: Recovery of the MBD-free spectrum based on synthetic data (step (d) in Fig. 5) as example for the 'forbidden' $LiTaO_3$ 0 3 15 reflection. Different threshold values to discriminate MDB-contribution are chosen. The "lowest i%" data are the mean of values below the i^{th} percentile of intensity $I_E(\psi)$ at a given energy. The lowest 100 % data set represents the overall mean. Additionally, the median (50^{th} percentile) is shown. Please note the different scales of the y axis. Bottom: Relative differences between original (fdmnes) and restored signal $(I_{\text{r}} - I_{\text{o}})/I_{\text{o}}$.

5. Conclusion and Outlook

We presented an automatable approach to receive clean, Renninger reflection free, REX spectra. The employed approach requires establishing scans of the azimuthal angle ψ, e.g. as a virtual motor in the beamline control. Subsequently, ψ-E grids are measured with a finely screened azimuthal angle in the inner loop and moderately stepped energies in the outer one. Employing a python script, the detector frames

corresponding to a ψ-E grid are handled and energy dependent signal and background are returned, free from the Renninger Effect. As a result, clean REX spectra can be measured even at relatively high energies with respect to the unit cell dimensions (see Fig. 6), which, in turn, allows to study anomalous diffraction from crystals at absorption edges located at high energies. Moreover, this facilitates the study of local structure and chemical environment of an extendet set of chemical elements in highly perfect single-crystals of materials. The successful recovery of the REX spectra is mainly limited by the density of the multiple beam cases: if the density is very low, no recovery is needed as the data is not strongly affected. This is often the case for low energies, small unit cells, and also for weakly scattering samples (*e. g.* powders, thin films) and low excitation errors. If the density becomes higher, a recovery is possible if still some angular ranges exist that are relatively unaffected from MBD. Otherwise, the presented approach will also fail. Our approach is especially beneficial for the investigation of 'forbidden' reflections, which are particularly sensitive to the Renninger Effect. We have demonstrated the effectiveness of the procedure on the energy-dependence of the forbidden 0 3 15 reflection of $LiTaO_3$ near the Ta L_3 edge.

Acknowledgements. We acknowledge DESY (Hamburg, Germany), a member of the Helmholtz Association HGF, for the provision of experimental facilities. Parts of this research were carried out at PETRA III and we would like to thank Yury Matveev for assistance in using beamline P23. Beamtime was allocated for proposal I-20181183.

Funding Information. Financial support is cordially acknowledged during projects of Deutsche Forschungsgemeinschaft (DFG; REXSuppress 324641898 and AcoustREXS 409743569). Part of the work was conducted within the EURIZON project (formerly CREMLINplus), which received funding from the European Union's Horizon 2020 research and innovation programme under grant agreement No. 871072. The beamtime

was reimbursed by DESY Photon Science (bursary No. I-20181183).

References

[1] A. Authier. *Dynamical Theory of X-ray Diffraction*, volume 11. Oxford University Press on Demand, 2005.

[2] B. W. Batterman and H. Cole. Dynamical Diffraction of X Rays by Perfect Crystals. *Reviews of Modern Physics*, 36:681, 1964.

[3] M. Renninger. "Umweganregung", eine bisher unbeachtete Wechselwirkungserscheinung bei Raumgitterinterferenzen. *Zeitschrift für Physik*, 106:141, 1937.

[4] M. Newville. Fundamentals of XAFS. Reviews in Mineralogy and Geochemistry, July 2021. `https://dictionary.iucr.org/Renninger_effect`.

[5] V. G. Kohn. On the Theory of the Bragg Reflection in the Case of Multiple X-Ray Diffraction. *Physica Status Solidi A*, 54:375, 1979.

[6] V. G. Kohn and A. Kazimirov. High-resolution study of (002, 113, 11$\bar{1}$) four-beam diffraction in Si. *Acta Crystallographica A*, 68:331, 2012.

[7] P. A. Besirganyan, R. T. Gabrielyan, V. G. Kohn, and A. H. Toneyan. Six-Beam X-Ray Diffraction in Ge Single Crystals. *Physica Status Solidi A*, 85(2):331, 1984.

[8] V. Holý, K. Wolf, M. Kastner, H. Stanzl, and Gebhardt W. X-ray triple-crystal diffractometry of defects in epitaxic layers. *Journal of Applied Crystallography*, 27:551, 1994.

[9] M. A. Krivoglaz. *X-ray and Neutron Diffraction in Nonideal Crystals*. Springer, 1996.

[10] H. J. Juretschke. Modified two-beam description of X-ray fields and intensities near a three-beam diffraction point. General formulation and first-order solution. *Acta Crystallographica A*, 40:379, 1984.

[11] R. T. Gabrielyan and V. G. Kohn. The forbidden-reflection method for absorption coefficient measurement in many-wave x-ray diffraction in single crystals. *Physica Status Solidi A*, 63(1):345, 1981.

[12] M. Richter, C. Zschornak, D. Novikov, E. Mehner, M. Nentwich, J. Hanzig, S. Gorfman, and D. C. Meyer. Picometer polar atomic displacements in strontium titanate determined by resonant X-ray diffraction. *Nature Communications*, 9:178, 2018.

[13] T. Weigel, C. Richter, M. Nentwich, E. Mehner, V. Garbe, L. Bouchenoire, D. Novikov, D. C. Meyer, and M. Zschornak. What is the origin of the ferroelectricity in the commensurate low temperature phase of YMn_2O_5? Physical Review X, 2023. (in progress).

[14] M. Nentwich, M. Zschornak, C. Richter, D. Novikov, and D. C. Meyer. Analysis of modulated Ho_2PdSi_3 crystal structure at Pd K and Ho L absorption edges using resonant elastic X-scattering. *Journal of Physics: Condensed Matter*, 28:066002, 2016.

[15] Y. Laligant and Y. Calage. Ordered magnetic frustration: VII. Na_2NiFeF_7: Reexamination of its Crystal Structure in the true Space Group after corrections from Renninger Effect and Refinement of its frustrated Magnetic Structure at 4.2 and 55 K. *Journal of Solid State Chemistry*, 78:66, 1989.

[16] J. Baruchel. *Neutron and Synchrotron Radiation for Condensed Matter Studies*, volume 1. Springer Verlag Berlin, 1993.

[17] W. Massa. *Kristallstrukturbestimmung*, volume 6. Springer, 2007.

[18] A. Petocv. *Röntgenographische Untersuchungen an Lithiumniobat, $LiNbO_3$: Auswirkungen der anisotropen chemischen Umgebung auf das Streuvermögen von Niob*. PhD thesis, Universität des Saarlandes, Saarbrücken, 7 1989. https://bib-pubdb1.desy.de/record/221685/files/DESY-HASYLAB-89-08.pdf.

[19] M. A. Hayashi, L. H. Avanci, L. P. Cardoso, J. Bettini, M. M. G. de Carvalho, Morelhão S. L., and S. P. Collins. High-resolution synchrotron radiation Renninger scan to examine hybrid reflections in InGaP/GaAs(001). *Journal of Synchrotron Radiation*, 6:29, 1999.

[20] A. O. dos Santos, R. Lang, J. M. Sasaki, and L. P. Cardoso. Assessment of phase transition and thermal expansion coefficients by means of secondary multiple reflections of Renninger scans. *Journal of Applied Crystallography*, 52:1271, 2019.

[21] M. Borcha, I. Fodchuk, M. Solodkyi, and M. Baidakova. Structure diagnostics of heterostructures and multi-layered systems by X-ray multiple diffraction. *Journal of Applied Crystallography*, 50:722, 2017.

[22] P. Mikula, J. Šaroun, P. Strunz, and V. Ryukhtin. Investigation of multiple Bragg reflections and their possible exploitation. *Journal of Neutron Research*, 23:29, 2021.

[23] R. O. Freitas, T. E. Lamas, A. A. Quivy, and S. L. Morelhão. Synchrotron X-ray Renninger scanning for studying strain in InAs/GaAs quantum dot system. *Physica Status Solidi*, 204:2548, 2007.

[24] S.-L. Chang. *X-ray multiple-wave diffraction: theory and application*, volume 143. Springer Science & Business Media, 2004.

[25] S.-L. Chang. Theoretical consideration of experimental methods for X-ray phase determination using multiple diffraction. *Acta Crystallogrpahica A*, 38:516, 1982.

[26] E. Weckert and K. Hümmer. Multiple-Beam X-ray Diffraction for Physical Determination of Reflection Phases and its Applications. *Acta Crystallographica A*, 53:108, 1997.

[27] M. Zschornak, C. Richter, M. Nentwich, H. Stöcker, S. Gemming, and D. C. Meyer. Probing a crystal's short-range structure and local orbitals by Resonant X-ray Diffraction methods. *Crystal Research and Technology*, 49:43, 2014.

[28] K. A. Kozlovskaya, A. G. Kulikov, D. Novikov, E. N. Ovchinnikova, A. M. Ustyugov, and V. E. Dmitrienko. Handling of Multiple-Wave Effects in the Measurement of Forbidden X-Ray Reflections in TeO_2. *Crystal Research and Technology*, 56:2000195, 2021.

[29] V. E. Dmitrienko. Multiwave diffraction, phase problem, and extinction in imperfect crystals. *Crystallography Reports*, 54:985, 2009.

[30] E. Ovchinnikova, D. Novikov, M. Zschornak, A. Kulikov, K. Kozlovskaya, V. Dmitrienko, A. Oreshko, A. Blagov, E. Mukhamedzhanov, N. Marchenkov, M. Borisov, A. Khadiev, A. Petrenko, and Y. Pisarevsky. Forbidden Reflections in TeO_2 in the Vicinity of the Te L_1 Absorption Edge. *Crystals*, 10:719, 2020.

[31] C. Richter. pyasf – python module to compute the anisotropic resonant scattering factor. https://github.com/carichte/pyasf/releases, 2021.

[32] B. Walz. *Determination of dopant atomic positions with kinematical X-ray standing waves*. PhD thesis, Deutsches Elektronen-Sychrotron, Universität Hamburg, 2011. https://inis.iaea.org/search/search.aspx?orig_q=RN:43003536.

[33] S. C. Abrahams, J. M. Reddy, and J. L. Bernstein. Ferroelectric lithium tantalate. 1. Single crystal X-ray diffraction study at 24 °C. *Journal of Physics and Chemistry of Solids*, 28:1685, 1967.

[34] R. T. Smith and F. S. Welsh. Temperature Dependence of the Elastic, Piezoelectric, and Dielectric Constants of Lithium Tantalate and Lithium Niobate. *Journal of Applied Physics*, 42:2219, 1971.

[35] T. Köhler, E. Mehner, J. Hanzig, G. Gärtner, H. Stöcker, T. Leisegang, and D. C. Meyer. Real structure influencing the hydrogen defect chemistry in congruent $LiNbO_3$ and $LiTaO_3$. *Journal of Solid State Chemistry*, 244:108, 2016.

[36] T. Köhler, E. Mehner, J. Hanzig, C. Gärtner, G. Funke, Y. Joseph, T. Leisegang, H. Stöcker, and D. C. Meyer. Kinetics of the hydrogen defect in congruent $LiMO_3$. *Journal of Materials Chemistry C*, 9:2360, 2021.

[37] M. U. de Vivanco, M. Zschornak, H. Stöcker, S. Jachalke, E. Mehner, T. Leisegang, and D. C. Meyer. Pyroelectrically-driven chemical reactions described by a novel thermodynamic cycle. *Physical Chemistry Chemical Physics*, 22:17781, 2020.

[38] R. L. Barns and J. R. Carruthers. Lithium tantalate single crystal stoichiometry. *Journal of Applied Crystallography*, 3(5):395, 1970.

[39] S. Miyazawa and H. Iwasaki. Congruent melting composition of lithium metatantalate. *Journal of Crystal Growth*, 10(3):276, 1971.

[40] C. D. Brandle and D. C. Miller. Czochralski growth of large diameter $LiTaO_3$ crystals. *Journal of Crystal Growth*, 24:432, 1974.

[41] Y. Furukawa, K. Kitamura, E. Suzuki, and K. Niwa. Stoichiometric $LiTaO_3$ single crystal growth by double crucible Czochralski method using automatic powder supply system. *Journal of crystal growth*, 197(4):889, 1999.

[42] A. Vyalikh, M. Zschornak, T Köhler, M. Nentwich, T. Weigel, J. Hanzig, R. Zaripov, E. Vavilova, S. Gemming, E. Brendler, and D. C. Meyer. Analysis of the defect clusters in congruent lithium tantalate. *Physical Review Materials*, 2:013804, 2018.

[43] N. Zotov, H. Boysen, F. Frey, T. Metzger, and E. Born. Cation substitution models of congruent $LiNbO_3$ investigated by X-ray and neutron powder diffraction. *Solids*, 55:145, 1994.

[44] T. Köhler, M. Zschornak, M. Zbiri, J. Hanzig, C. Röder, C. Funke, H. Stöcker, E. Mehner, and D. C. Meyer. Defect formation in chemically reduced congruent $LiTaO_3$: ab initio simulations and inelastic neutron scattering. *Journal of Materials Chemistry C*, 9:13484, 2021.

[45] T. Köhler, M. Zschornak, C. Röder, J. Hanzig, G. Gärtner, T. Leisegang, E. Mehner, H. Stöcker, and D. C. Meyer. Chemical environment and occupation sites of hydrogen in $LiMO_3$. *Journal of Materials Chemistry C*, 11:520, 2023.

[46] H. Bethe. Theorie der Beugung von Elektronen an Kristallen. *Annalen der Physik*, 392(17):55, 1928.

[47] C. Richter, D. V. Novikov, E. K. Mukhamedzhanov, M. M. Borisov, K. A. Akimova, E. N. Ovchinnikova, A. P. Oreshko, J. Strempfer, M. Zschornak, E. Mehner, D. C. Meyer, and V. E. Dmitrienko. Mechanisms of the paraelectric to ferroelectric phase transition in RbH_2PO_4 probed by purely resonant x-ray diffraction. *Physical Review B*, 89:094110, 2014.

[48] D. Schwarzenbach and H. D. Flack. On the definition and practical use of crystal-based azimuthal angles. *Journal of Applied Crystallography*, 22:601, 1989.

[49] O. Bunău and Y. Joly. Self-consistent aspects of x-ray absorption calculations. *Journal of Physics: Condensed Matter*, 21:345501, 2009.

Synopsis

An approach is presented to reliably extract the desired intensities and to filter out Multiple Beam X-ray Diffraction, which often interferes for high X-ray energies and for large unit cells. Here, a universal concept of data acquisition and post processing for resonant X-ray diffraction experiments is presented; including the measurement of the energy dependent intensity at several azimuthal angles and subsequently only considering the unaffected data points.